IEEE Access
Multidisciplinary | Rapid Review | Open Access Journal

Received September 25, 2020, accepted October 12, 2020, date of publication October 15, 2020, date of current version August 31, 2021.

*Digital Object Identifier 10.1109/ACCESS.2020.3031284*

# Voltage Correlation Based Single Pole-to-Ground Fault Detection of MMC-HVDC Transmission Line

**NA AN[1,2], HONGCHUN SHU[1,2], (Member, IEEE), BO YANG[2], PULIN CAO[2], (Member, IEEE), JIAN SONG[1,2], AND YU GUO[1], (Member, IEEE)**

[1]Faculty of Mechanical and Electrical Engineering, Kunming University of Science and Technology, Kunming 650500, China
[2]Faculty of Electric Power Engineering, Kunming University of Science and Technology, Kunming 650500, China

Corresponding author: Jian Song (kustsj2018@126.com)

This work was supported by the National Natural Science Foundation of China under Grant 52037003 and Grant 51807085.

**ABSTRACT** Through analysis of various fault voltage characteristics of modular multilevel converter high voltage direct current (MMC-HVDC) transmission system, it shows that the positive and negative voltage relationships of direct current transmission lines with single pole-to-ground faults are obviously different from other faults. Hence, Pearson correlation coefficient is used to describe the degree of difference in this work. In the case of single pole-to-ground fault, correlation coefficient is positive and close to 1, while as for other failures, correlation coefficient is negative and close to −1. This article analyzes the mechanism of correlation coefficient to withstand transition resistance and verifies the effectiveness of the proposed method under high resistance grounding fault. A novel scheme is proposed by combining the quantity sum of voltage variation characteristics, which can effectively identify fault pole. The proposed scheme needs smaller time window and owns high efficiency, as well as great robustness to transition resistance.

**INDEX TERMS** MMC-HVDC transmission, high resistance ground fault, Pearson correlation coefficient, fault detection.

## I. INTRODUCTION

At present, high-voltage direct-current (HVDC) long-distance transmission lines have gained ever-growing attentions around the globe for the sake of significant renewable energy integration into main power grid, such as wind [1] and solar [2]. The power industry requires a dramatic safe and stable operation [3]–[5]. One of the crucial tasks of HVDC system is to accurately and reliably identify transmission line faults [6]–[8].

Compared with traditional HVDC system, modular multilevel converter (MMC) HVDC system owns numerous advantages, such as no reactive compensation or commutation failure, independent regulation of active and reactive power, and ability to supply power to passive systems, etc.. MMC has become a research hotspot due to the above advantages [9]–[12]. HVDC transmission line protection is one of the crucial technical problems that MMC-HVDC transmission system needs to solve. Since the topology of MMC and operation mechanism of sub-modules are quite different from traditional HVDC, MMC-HVDC transmission line protection methods can refer to traditional HVDC transmission line protection method, but not all methods which are applicable to traditional HVDC transmission line protection are applicable to MMC-HVDC transmission line. Compared with two-level and three-level voltage source converter (VSC) [13]–[16], fault transient characteristics of flexible direct-current (DC) transmission system are obviously different as modular multilevel converter has no parallel capacitor on its DC side. Therefore, based on the characteristics of MMC-HVDC transmission system, it is necessary to investigate suitable fault detection method to enhance security and stability of power systems.

HVDC transmission line protection [17]–[20] mainly includes traveling wave protection, DC undervoltage protection, differential protection, etc., among which traveling wave protection is the main protection and others are backup ones. Traveling wave protection and DC undervoltage protection are easy to be rejected when high resistance ground fault occurs. The time of differential protection is prolonged, so it is difficult to execute backup protection [21]–[24]. To solve these problems, many improvements have been designed to protect flexible DC transmission lines. Reference [25] proposed a novel single-ended transient-voltage-based

The associate editor coordinating the review of this manuscript and approving it for publication was Amedeo Andreotti.

protection strategy, which used wavelet transform to extract transient voltage energy. In [26], an online detection and protection method based on graph theory is proposed for fault-line selection and fault-type identification. However, several problems still exist, such as poor robustness to transition resistance and easy to be disturbed [27]–[29].

For overhead transmission lines of MMC-HVDC, the probability of single pole-to-ground (PG) fault is relatively high [10]. The fault current is small, which is difficult to be rapidly identified if a single PG fault occurs. After the transient, fault pole voltage is reduced to zero, the amplitude of non-fault pole voltage is doubled. In consequence, it requires high insulation level of HVDC transmission lines. Hence, it is considerably significant to rapidly identify single pole-to-ground faults, which can alarm operators for potential threats or events of MMC-HVDC system. The bipolar short-circuit fault is the most serious fault in MMC-HVDC transmission system. The voltage of positive and negative poles decrease, voltage between poles also decreases. The fault current is large, which is easy to be rapidly identified if bipolar short-circuit fault occurs.

Thus far, there are few studies on single PG faults in MMC-HVDC system. Literature [10] proposed a fault location method using active pulse. Reference [30] distinguished between temporary faults and permanent faults by signal injection. Moreover, an adaptive re-closing scheme applied to the MMC system was proposed by injecting voltage pulses to faulty lines [31], which however ignores to identify single PG faults in a short time. Generally speaking, fault current is quite small in high resistance fault, thus work [32] was inadequate to withstand transition resistance. Besides, an equivalent transient characteristics calculation method was designed for PG faults [33], which calculation time range is 20 ms. Meanwhile, an effective algorithm was developed to detect single PG faulty feeder based on capacitance to ground of zero-mode fault network of radial MVDC system [34]. Lastly, a novel capacitance fuzzy identification method [35] was designed to identify single PG fault with the requirement of reliable and accurate communication.

Combined with structural characteristics of MMC system, this article analyzes positive and negative pole voltage characteristics of HVDC transmission line fault, and studies the correlation characteristics between these two poles. Based on correlation between positive and negative voltages of MMC-HVDC transmission lines, a novel voltage correlation based single PG fault detection is proposed, which owns strong robustness. In particular, it can effectively identify high resistance ground fault, upon which the fault current is insignificant and difficult to identify by other alternatives. In addition, voltage correlation can satisfactorily operate without any filtering.

The remaining of this article is organized as follows: MMC-HVDC modelling is presentation in Section 2. Section 3 is devoted to analysis correlation between positive and negative voltages of a single PG fault, while several other types of faults are analyzed in Section 4. Then, in Section 5, characteristics of voltage correlation are analyzed. In Section 6, fault detection algorithm for single PG of transmission line is proposed. At last, some conclusions are summarized in Section 7.

## II. MMC-HVDC MODELLING

MMC-HVDC transmission system is composed of MMC converter stations and DC transmission lines. The structure (symmetrical monopole configuration) of MMC-HVDC (77 levels) transmission system is demonstrated in Fig. 1. Here, active networks are used in alternating current (AC) systems at both converter stations, while an equivalent model of AC system with frequency of 50 Hz and a rated voltage of 230 kV is adopted. Triangle connection is adopted by side winding of the connecting transformer valve without neutral point, while star connection is adopted by AC side of the connecting transformer, and the neutral point is grounded directly. The connecting transformer ratio is 230kV/370kV, with a leakage reactance of 0.1 p.u.. In addition, DC bus is grounded by a clamping resistance ($R_d$) with a large value, and its main function is to provide pole voltages of clamping and zero potential reference point of direct current system in normal operation [36]. The HVDC transmission line (without smoothing reactor) is 400 km with the rated DC voltage being $\pm$320 kV and rated power being 1200 MVA. In Fig. 1, $u_{Rn}$ and $u_{Rp}$ are the negative and positive voltage on rectifier side, while $u_{In}$ and $u_{Ip}$ are the negative and positive voltage on inverter side. $i_{Rn}$ and $i_{Rp}$ are negative and positive currents on rectifier side, while $i_{In}$ and $i_{Ip}$ are negative and positive currents on inverter side, respectively. The current direction reference is shown in Fig. 1. G1 and G2 are sending and receiving terminal of AC system while T1 and T2 are converter transformers.

The classical half-bridge sub-module (SM) MMC is used as basic converter topology, as shown in Fig. 1. Half - bridge sub-modules MMC are more economical than full - bridge structures and hybrid structures. The bridge arm inductance $L_0 = 50$mH and the sub-module capacitance $C_0 = 2800\mu$F. The inter-polar voltage is denoted as $u_{dc}$. When MMC transmission system operates normally, positive and negative voltage on rectifier side respectively can be calculated by

$$u_{Rp} = \frac{1}{2}u_{dc} \tag{1}$$

$$u_{Rn} = -\frac{1}{2}u_{dc} \tag{2}$$

## III. SINGLE POLE-TO-GROUND FAULT ANALYSIS

### A. FAULT CURRENT

In transmission system illustrated in Fig. 1, direct current buses are respectively grounded by two large resistors, which can clamp pole voltages to provide zero potential reference points for MMC-HVDC system. If a single PG fault occurs, there is no connection point to the ground at both ends of DC valve side because of their triangular wiring. Moreover, because the clamping resistance has a great value, it can

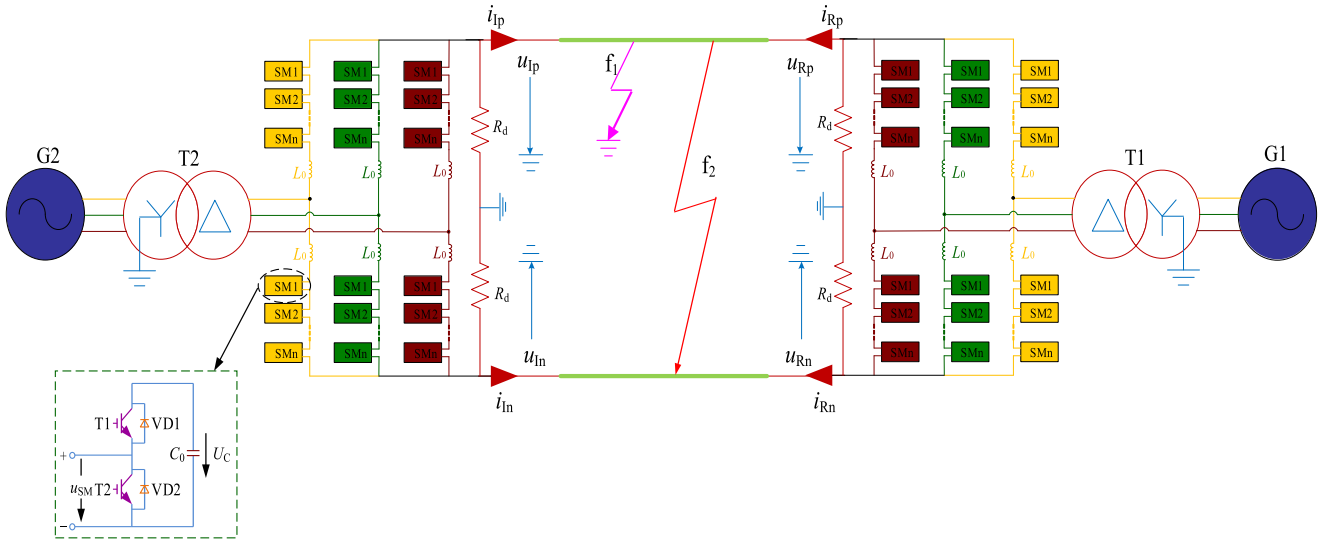


**FIGURE 1.** Schematic diagram of an MMC-HVDC transmission system.

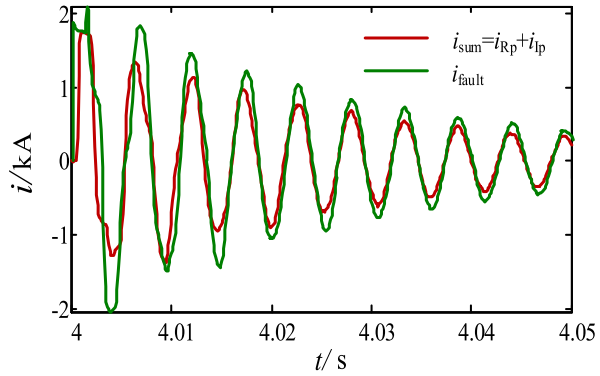


**FIGURE 2.** Fault current comparison.

be considered as open circuit if a single PG fault occurs. In theory, for alternating current system, it only changes the electric potential reference point in DC system, which can still transmit power [36].

If there is a single PG fault ($f_1$) in the system, a path will be formed by distributed capacitance of non-fault line, fault line and converter station for the transient current after fault line is grounded by a resistance $R_f$ [37]. It is shown from the simulation that the current flowing from negative pole to fault point coincides with that flowing from fault point to positive pole, which well matches the theoretical analysis. As depicted in Fig. 2, current of positive pole line at both ends is basically consistent with the measured current at fault point ($i_{fault}$) that is slightly larger than the sum of current ($i_{sum}$) at both ends. Because the distributed capacitance conduction on transmission line provides a path for part of fault current, but the current does not pass through the measured point at both ends.

### B. FAULT VOLTAGE

In MMC-HVDC transmission system, fault current is set as $i_f$, $R_{xf}$ and $L_{xf}$ as resistance and inductance from outlet of rectifier side to fault point of transmission line, $i_{Rp}$ as positive pole line current, and the positive pole voltage $u_{Rp}$ is described as

$$u_{Rp} \approx i_f R_f + i_{Rp} R_{xf} + L_{xf} \frac{di_{Rp}}{dt} \tag{3}$$

In Eq. (4), $u_{dc}$ is voltage between positive and negative poles when fault occurs, and the negative voltage is calculated as follows:

$$u_{Rn} \approx (i_f R_f + i_{Rp} R_{xf} + L_{xf} \frac{di_{Rp}}{dt}) - u_{dc} \tag{4}$$

According to previous analysis of fault current, the distributed capacitance conduction on transmission line forms a path for part of fault current, which does not pass through the measured point. Therefore, $i_{Rp}$ measured at the terminal near rectifier is less than the current on actual line, and the current is not the same in different positions. Therefore, there is a calculation error in calculating voltage by measuring the current $i_{Rp}$, and the above equation can only be used as an approximate sign.

If a positive PG fault at 180km occurs in MMC-HVDC system, the fault voltage $u_{dc}$, $u_{Rp}$ and $u_{Rn}$ are shown in Fig. 3. The change laws of positive and negative voltage are the same. It can be seen from that voltage $u_{dc}$ between positive and negative poles oscillates in initial stage of the fault, but its amplitude and frequency of oscillation are much smaller than that of the unipolar voltage, and voltage value is stable around steady-state value. While unipolar voltage oscillates significantly, which positive voltage decreases to 0 and negative voltage is clamped to double after transient state.

### C. VOLTAGE CORRELATION ANALYSIS

Based on the analysis of voltage characteristics of single PG fault in MMC-HVDC transmission system, positive and negative voltages can be expressed by Eqs. (3) and (4). It can

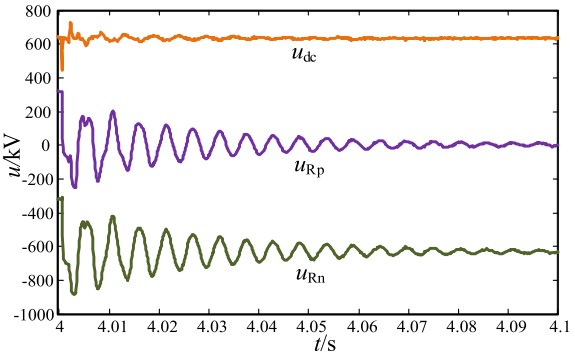


**FIGURE 3.** DC transmission line voltage with single PG fault.

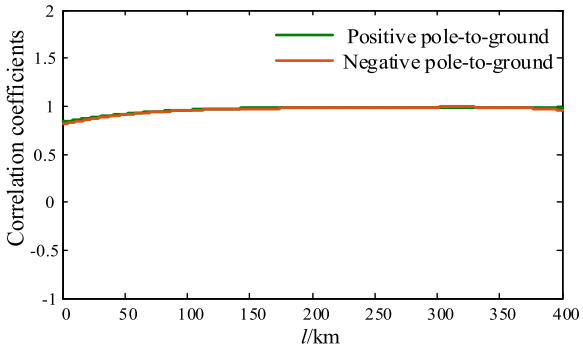


**FIGURE 4.** The voltage correlation coefficient of single PG faults.

be seen that their relationship satisfies the followings:

$$u_{\mathrm{Rn}} = u_{\mathrm{Rp}} - u_{\mathrm{dc}} \tag{5}$$

The correlation coefficient can be used to measure the similarity between positive and negative voltages of HVDC transmission lines. Here, covariance and variance are adopted to measure the correlation degree of two variables in Person correlation coefficient. And it is not affected by the amplitude of variable [38]. Person correlation coefficient can effectively measure the similarity between positive and negative voltage. For convenience of expression, let $u = u_{\mathrm{Rp}}$ and $v = u_{\mathrm{Rn}}$, then the discrete expression is described as

$$\rho(u, v) = \frac{\sum_{i=1}^{n}(u_i - \frac{1}{n}\sum_{j=1}^{n}u_j)(v_i - \frac{1}{n}\sum_{j=1}^{n}v_j)}{\sqrt{\sum_{i=1}^{n}(u_i - \frac{1}{n}\sum_{j=1}^{n}u_j)^2}\sqrt{\sum_{i=1}^{n}(v_i - \frac{1}{n}\sum_{j=1}^{n}v_j)^2}} \tag{6}$$

where, $u$ and $v$ are respectively positive and negative voltage, $u = \{u_1, u_2, \ldots, u_n\}$, $v = \{v_1, v_2, \ldots, v_n\}$, which are two different variables, and n is the number of sampling points. Here, $i = 1, 2, \ldots, n$ and $j = 1, 2, \ldots, n$.

If these two different variables, e.g., $u$ and $v$, satisfy

$$v = u + c \tag{7}$$

where c is constant. The correlation coefficient is $\rho(u, v) = 1$.

If these two different variables, $u$ and $v$, satisfy

$$v = -u \tag{8}$$

The correlation coefficient is $\rho(u, v) = -1$.

The correlation coefficient $\rho(u, v) = 1$ indicates that change laws of $u$ and $v$ are identical, whose waveforms are completely similar, and the positive correlation is the strongest. The correlation coefficient $\rho(u, v) = -1$ indicates that the change laws of $u$ and $v$ are absolutely opposite. The represented waveforms are described as negative and completely similar with some axial symmetry. If the absolute value of correlation coefficient approaches to zero, the change laws of these two variables are fairly diverse. There is a low degree of correlation between these two variables, whose waveforms have no resemblance.

According to the voltage relationship of two poles and the expression of correlation coefficient, it can be known that the similarity of positive and negative voltage depends on inter-electrode voltage $u_{\mathrm{dc}}$. If inter-polar voltage $u_{\mathrm{dc}}$ is constant, correlation coefficient of $u_{\mathrm{Rp}}$ and $u_{\mathrm{Rn}}$ can be calculated according to Person correlation coefficient, that is, the change rules of positive and negative voltage are exactly identical, the strongest correlation is positive, and the positive and negative voltage waveforms are completely resemble. In this case, it can be considered that the positive line voltage waveform is negative line voltage waveform after $u_{\mathrm{dc}}$ is moved down along the vertical axis. In fact, inter-pole voltage $u_{\mathrm{dc}}$ fluctuates slightly at the moment of failure, and the transient process is short but exists, as demonstrated in Fig. 3. The inter-polar voltage $u_{\mathrm{dc}}$ is not a completely constant value and can only be approximately considered to be close to a constant value to a certain extent. The change laws of $u_{\mathrm{Rp}}$ and $u_{\mathrm{Rn}}$ are almost identical, whose waveforms are quite similar and positively correlated. Thus, correlation coefficient between $u_{\mathrm{Rp}}$ and $u_{\mathrm{Rn}}$ is close to, but not equal to 1.

Therefore, the correlation coefficient between positive and negative voltage approaches to 1 after the occurrence of a single PG fault. The distribution characteristics of correlation coefficient along the whole line are shown in Fig. 4. Whether a positive or negative PG fault occurs, the voltage correlation is positive, and the correlation coefficient approaches to 1.

## IV. ANALYSIS OF OTHER FAULTS

### A. BIPOLAR SHORT-CIRCUIT FAULT

#### 1) FAULT FEATURES

The bipolar short-circuit fault, as shown in Fig. 1 ($f_2$), is the most serious fault in MMC-HVDC transmission system, which is equivalent to a three-phase short circuit fault in AC system. The voltage of positive and negative poles decrease, voltage between poles also decreases. And the decreased amplitude is relevant to transition resistance in short circuit. In case of metallic short-circuit, voltage amplitude decreases to 0. The fault circuit of bipolar short-circuit are converter station, positive pole line and negative pole line. While the main fault circuit of single PG are distributed capacitance of non-fault pole, fault pole, and converter station. When a bipolar short-circuit fault occurs, discharging current of distributed

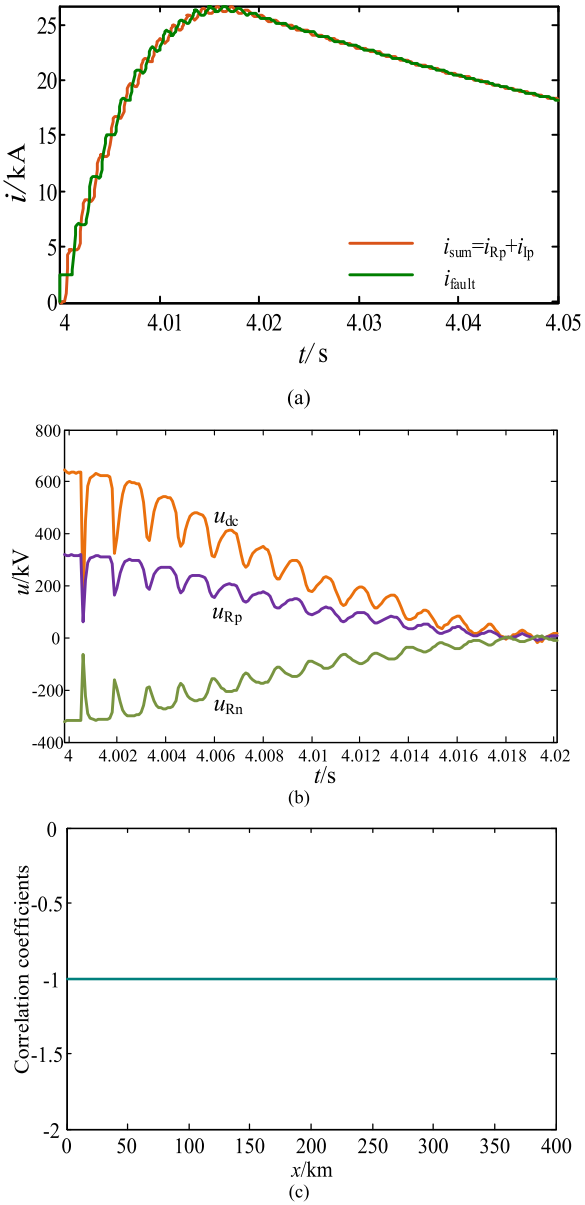


**FIGURE 5.** Bipolar short-circuit fault. (a) Fault current comparison. (b)Voltage of dc transmission line with bipolar short-circuit. (c)The voltage correlation coefficient of bipolar short-circuit.

capacitance of transmission line is far less than that of short circuit fault current, so there is a slight difference between calculated fault current at both ends and measured current at fault point. But their difference is very small, as shown in Fig. 5(a). It is obvious that these two currents are mostly the same, with little difference in value, which is consistent with the above theoretical analysis. This is very different from the single PG fault.

Suppose fault current is $i_f$, $R_f$ is short-circuit point transition resistance, $R_{xf}$ and $L_{xf}$ are resistance and inductance from rectifier side outlet to the fault point, $i_{Rp}$ is positive pole line current on rectifier side, $i_{Rn}$ is negative pole line current on rectifier side, and the inter-pole voltage $u_{dc}$ is described as

$$u_{dc} = i_f R_f + (i_{Rp} - i_{Rn})R_{xf} + L_{xf}\left(\frac{di_{Rp}}{dt} - \frac{di_{Rn}}{dt}\right) \quad (9)$$

Positive voltage $u_{Rp}$ and negative voltage $u_{Rn}$ are respectively described as

$$u_{Rp} = \frac{1}{2}u_{dc} \quad (10)$$

$$u_{Rn} = -\frac{1}{2}u_{dc} \quad (11)$$

Fig. 5(b) shows variation of DC transmission line voltage after the occurrence of bipolar metallic short-circuit fault. It can be found that after a period of transient change, the voltage amplitude drops to 0. The transient process of positive and negative voltage is almost symmetric along zero axis of voltage.

#### 2) VOLTAGE CORRELATION ANALYSIS OF BIPOLAR SHORT-CIRCUIT FAULT

Bipolar short-circuit fault is serious, which positive and negative voltage expressions are shown in Eqs. (10) and (11). It can be seen that relationship of positive and negative voltage satisfies $u_{Rn} = -u_{Rp}$ and correlation coefficient -1 can be obtained by substituting it into Person correlation coefficient (6). It is shown that the positive and negative voltage changes are completely opposite, and the correlation is the strongest with negative. The voltage waveform of two poles are described as negative similarity with zero axial symmetry. The distribution characteristics of correlation coefficient along the whole line are illustrated in Fig. 5(c).

It is obvious that the correlation coefficients of positive and negative voltage in bipolar short-circuit faults are $-1$, which are consistent with the theoretical analysis. It shows that positive and negative voltage have strong negative correlation and the waveforms are almost symmetric along the zero axis.

### B. ANALYSIS OF AC SIDE FAULT VOLTAGE CHARACTERISTICS

#### 1) FAULT FEATURES

In the case of AC side failure, voltage transient process at observation point of direct current transmission line is relatively insignificant due to the existence of components such as converter transformer, converter station sub-module capacitance, bridge arm reactor, etc.. After the failure of AC side of MMC system, DC side no longer outputs relatively stable DC voltage, instead outputs voltage that changes significantly over time. The positive voltage $u_{Rp}$ and negative voltage $u_{Rn}$ also satisfy Eqs. (10) and (11). After a three-phase short circuit fault occurs at rectifier side, measured voltage transient process is shown in Fig. 6.

#### 2) VOLTAGE CORRELATION ANALYSIS OF AC SIDE FAULT

When a fault occurs at AC side, the relation between positive and negative voltages also satisfies $u_{Rn} = -u_{RP}$, which is substituted into Person correlation coefficient (6). Similarly, their correlation coefficient is $-1$. It is shown that positive and negative voltage changes are completely opposite, and the correlation is the highest with negative. The voltage waveforms of the two poles are described as negative similarity

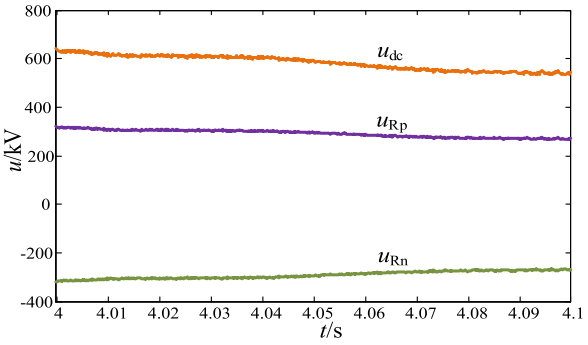


**FIGURE 6.** Voltage of DC transmission line with AC side fault.

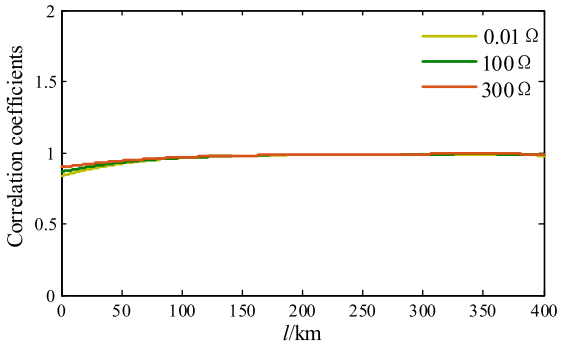


**FIGURE 7.** Correlation coefficients of different transition resistors for single pole-to-ground faults.

**TABLE 1.** Correlation between positive and negative voltage of AC side Faults.

| Fault location | Fault types | Correlation coefficient |
|---|---|---|
| Rectifier side | Three phase short circuit | -1 |
| Rectifier side | Two-phase-ground short circuit | -1 |
| Inverter side | Single-phase-ground short circuit | -1 |
| Inverter side | Three phase short circuit | -1 |

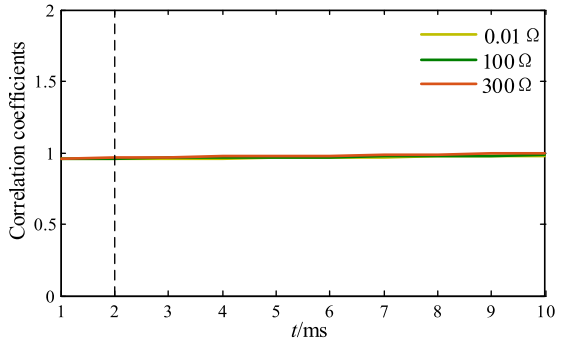


**FIGURE 8.** Correlation coefficients under different sampling Windows.

with zero axial symmetry. Some AC side faults correlation coefficients are shown in Table 1.

Table 1 reveals that correlation coefficients are −1, which indicates that a strong negative correlation exists between positive and negative voltages, and the waveform is symmetric along zero axis.

## V. CHARACTERISTICS OF VOLTAGE CORRELATION ANALYSIS

### A. ANALYSIS OF RESISTANCE TO TRANSITION RESISTANCE

According to Eqs. (3)-(5), magnitude of transition resistance $R_f$ affects the positive and negative voltages, but has little influence on their relationship. The transition resistance will affect the magnitude of inter-electrode voltage $u_{dc}$. The greater a transition resistance is, the smaller the transient impact of $u_{dc}$ will be, that is, the more constant inter-electrode voltage $u_{dc}$ tends to be. According to previous analysis, when transition resistance increases, the correlation coefficient between positive and negative voltage does not change significantly. Taking the above model as an example, the correlation coefficients between positive and negative voltage in different transition resistances are illustrated in Fig. 7.

Here, the correlation coefficients are positive and close to 1, with little change when transition resistance increases. The results show that positive and negative voltage have strong positive correlation, waveform similarity is very high, and they have enhanced ability to withstand transition resistance. Therefore, when MMC-HVDC transmission lines have high resistance single PG fault, the proposed method is still effective.

### B. SAMPLING TIME WINDOW

In the case of single PG fault, it can be seen from the relation between positive and negative voltages that they approximately satisfy Eq. (5). The correlation coefficient between the two depends on inter-electrode voltage $u_{dc}$. If inter-electrode voltage tends to a constant, the correlation coefficient between positive and negative voltage equals to 1. According to previous analysis, $u_{dc}$ is a non-constant, and the fault transient process has fluctuations. It can be seen that the correlation coefficients between positive and negative voltage are close to 1, but not equal to 1. As also from the correlation coefficient and the relationship between positive and negative voltage, the correlation coefficient is positive and close to 1, that is, a positive number less than 1. Since inter-electrode voltage fluctuates at the beginning of fault, data within 1ms and 10ms has little impact on the correlation coefficient, that is, the size of the sampling window has little impact on the correlation coefficient within a certain range. In the same fault location, with different transition resistance (0.01Ω, 100Ω and 300Ω), the correlation coefficients under different sampling time window are shown in Fig. 8. It can be seen that the correlation coefficient is slightly smaller when sampling window is 1ms, but there is little difference, which is between 0.95 to 1.0. The change of 1 ms to 2 ms is relatively obvious, but it is comparatively stable after 2 ms. The short window does not affect the identification, which does not require a specific sampling window. The window length can be selected according to the actual needs under the condition of satisfying the reliability.

The short window of sampling generally requires a higher sampling frequency to obtain sufficient information. However, a sampling frequency of 10 kHz is adopted in the proposed scheme, while no excessive requirement is needed for sampling channels.

## VI. FAULT DETECTION FOR SINGLE POLE-TO-GROUND OF TRANSMISSION LINES

### A. SETTING VALVE

Through analysis of various voltage characteristics and correlation between positive and negative voltage, it is found that the voltage characteristics of single PG faults are obviously different from other kinds of faults. In the case of single PG fault, positive and negative voltage variation rules have a strong positive correlation, and their waveforms similarity are extremely high, whose correlation coefficient are close to 1. In the case of bipolar short-circuit fault and AC side system failure, positive and negative voltage variation rules have a strong negative correlation, whose waveforms are almost symmetric along the zero axis, with the correlation coefficients being close to $-1$. Thus, the difference of the correlation coefficients between positive and negative voltage can be used to identify single PG faults. As shown from Fig. 4, the correlation coefficient of proximal single PG fault is small, with the correlation coefficient $\rho > 0.8$. Consider various practical factors, measurement errors, and a certain margin, reliability coefficient $K_{rel} = 1.2$ to 1.3 is chosen. Hence, the setting value of correlation coefficient $\rho_{set}$ is calculated as

$$\rho_{set} = \frac{\rho_{min}}{K_{rel}} = 0.6 \tag{12}$$

If the correlation coefficient is greater than $\rho_{set}$, it is considered that a single PG fault occurs. Otherwise, it is determined as other scenario.

### B. FAULT POLE IDENTIFICATION

Due to single PG fault, the absolute value of fault pole voltage begins to decline, while the absolute value of non-fault pole voltage begins to rise. Thus, this article proposes a method to identify fault pole. $u_p$ is positive voltage and $u_n$ is negative voltage, while the rated voltages of positive and negative poles are $U_p$ and $U_N$ respectively, together with threshold $\varepsilon_0 = 0.06$. Then, the identification of positive and negative pole is described as

$$\begin{cases} \dfrac{u_p - U_p}{U_p} < -\varepsilon_0, & \text{and } \dfrac{u_n - U_n}{U_n} > \varepsilon_0, \\ & \text{positve PG fault} \\ \dfrac{u_p - U_p}{U_p} > \varepsilon_0, & \text{and } \dfrac{u_n - U_n}{U_n} < -\varepsilon_0, \\ & \text{negative PG fault} \end{cases} \tag{13}$$

For discrete sampling points, it is counted the quantity of sampling value greater than $\varepsilon_0$ or less than $-\varepsilon_0$, as shown in Eq. (14). And the quantity sum of voltage variation characteristics is shown in Eq. (15), as follows

$$N_{count,i}(j) = \begin{cases} -1 & \dfrac{u_i(j) - U_i}{U_i} < -\varepsilon_0 \\ 0 & -\varepsilon_0 < \dfrac{u_i(j) - U_i}{U_i} < \varepsilon_0 \\ 1 & \dfrac{u_i(j) - U_i}{U_i} > \varepsilon_0 \end{cases} \tag{14}$$

$$N_{sum,i} = \sum_{j}^{N} N_{count,i}(j) \tag{15}$$

where $N_{count,i}$ is used to represent calculated value of different characteristics of voltage, $i = p$ or n, $Ns_{um,i}$ is the quantity sum of voltage variation characteristics in the data window, respectively.

Then, the discrete expressions of positive and negative pole fault identification are

$$\begin{cases} N_{sum,p} < -1, & \text{and } N_{sum,n} > 1, \text{ positive PG fault} \\ N_{sum,p} > 1, & \text{and } N_{sum,n} < -1, \text{ negative PG fault} \end{cases} \tag{16}$$

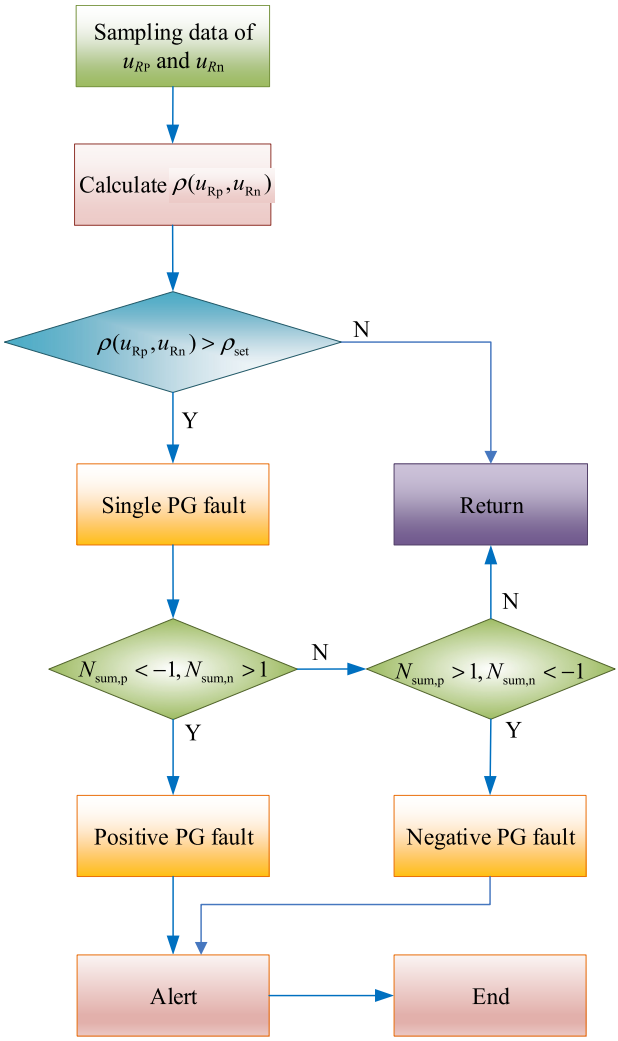


**FIGURE 9.** Flowchart.

**TABLE 2.** Fault identification results.

| Fault type | $x_f/\Omega$ | $x_f$/km | $\rho$ | Results |
|---|---|---|---|---|
| $L_p$-G | 0.01 | 80 | 0.9541 | Single PG fault |
| $L_p$-G | 0.01 | 140 | 0.9664 | Single PG fault |
| $L_p$-G | 0.01 | 180 | 0.9596 | Single PG fault |
| $L_p$-G (AWGN) | 0.01 | 180 | 0.9270 | Single PG fault |
| $L_p$-G | 0.01 | 280 | 0.9808 | Single PG fault |
| $L_p$-G (AWGN) | 0.01 | 280 | 0.9155 | Single PG fault |
| $L_p$-G | 100 | 160 | 0.9762 | Single PG fault |
| $L_p$-G | 100 | 380 | 0.9874 | Single PG fault |
| $L_p$-G (AWGN) | 100 | 380 | 0.9284 | Single PG fault |
| $L_p$-G | 300 | 240 | 0.9831 | Single PG fault |
| $L_p$-G | 1000 | 360 | 0.9828 | Single PG fault |
| $L_p$-G | 3000 | 20 | 0.8398 | Single PG fault |
| $L_n$-G | 1 | 300 | 0.9764 | Single PG fault |
| L-L | 1 | 140 | -1 | Others |
| L-L | 100 | 320 | -1 | Others |
| L-L | 300 | 340 | -1 | Others |
| R-AG | 1 | —— | -1 | Others |
| R-ABC | 0.01 | —— | -1 | Others |

**TABLE 3.** Fault pole identification.

| Fault type | $x_f/\Omega$ | $x_f$/km | $N_{sum,p}$ | $N_{sum,n}$ | Results |
|---|---|---|---|---|---|
| $L_p$-G | 0.01 | 80 | -28 | 28 | Positive PG fault |
| $L_p$-G | 0.01 | 140 | -29 | 28 | Positive PG faul |
| $L_p$-G | 0.01 | 180 | -28 | 27 | Positive PG faul |
| $L_p$-G (AWGN) | 0.01 | 180 | -28 | 27 | Positive PG faul |
| $L_p$-G | 0.01 | 280 | -28 | 26 | Positive PG faul |
| $L_p$-G (AWGN) | 0.01 | 280 | -28 | 27 | Positive PG faul |
| $L_p$-G | 100 | 160 | -28 | 27 | Positive PG faul |
| $L_p$-G | 100 | 380 | -28 | 24 | Positive PG faul |
| $L_p$-G (AWGN) | 100 | 380 | -28 | 26 | Positive PG faul |
| $L_p$-G | 300 | 240 | -28 | 26 | Positive PG fault |
| $L_p$-G | 1000 | 360 | -26 | 25 | Positive PG fault |
| $L_p$-G | 3000 | 20 | -28 | 20 | Positive PG fault |
| $L_n$-G | 1 | 300 | 26 | -28 | Negative PG fault |

### C. FLOWCHART

To sum up, voltage correlation coefficient is used to identify single PG faults, then the fault pole is identified according to the quantity sum of voltage variation. The overall flowchart is illustrated in Fig. 9.

### D. SIMULATION VERIFICATION

The proposed scheme is verified on PSCAD simulation platform with a sampling frequency of 10 kHz and data length of 3ms. Several case studies are carried out, while some simulation results are tabulated in Table 2. Here, $L_p$-G stands for positive PG fault, $L_p$-G(AWGN) for positive PG fault added white gaussian noise, $L_n$-G for negative PG fault, L-L for bipolar short-circuit fault, R-AG for single-phase grounding fault on rectifier side, R-ABC for three-phase short circuit fault on rectifier side, $R_f$ for transition resistance, $x_f$ for fault distance, $\rho$ for correlation coefficient, respectively.

Table 2 verifies the effectiveness of the proposed method, which has a strong ability to withstand transition resistance. In Table 3, it can be seen that the proposed method can correctly identify fault pole. They are consistent with theoretical analysis.

## VII. CONCLUSION

The distributed capacitance of non-fault pole and fault pole will form a path for transient current after fault pole is grounded due to distributed capacitance of transmission line if MMC-HVDC transmission system has a single PG fault. In the case of single PG fault, the relationship between positive and negative voltage is analyzed, which is found that the two are positive correlation and the waveforms are very similar. While other faults occur, the relationship between positive and negative voltage is negative correlation, whose waveforms are almost symmetric along the zero axis.

Person correlation coefficient between positive and negative voltages is adopted to identify single PG fault, which has high reliability and sensitivity. The data window length of proposed method is only 3ms. Moreover, the detection of single PG fault by voltage correlation has strong ability to withstand transition resistance, which provides theoretical support for detection of high-resistance grounding fault.

Lastly, fault poles are identified according to the characteristics of positive and negative voltage variations and quantitative polarity. The data window is consistent with data window of Person correlation coefficient to rapidly identify single PG fault. This method and voltage correlation cooperate to effectively identify single PG fault and select the fault which has extremely strong ability to withstand transition resistance.

## REFERENCES

[1] B. Yang, J. Wang, X. Zhang, T. Yu, W. Yao, H. Shu, F. Zeng, and L. Sun, "Comprehensive overview of meta-heuristic algorithm applications on PV cell parameter identification," *Energy Convers. Manage.*, vol. 208, Mar. 2020, Art. no. 112595.

[2] B. Yang, T. Yu, X. Zhang, H. Li, H. Shu, Y. Sang, and L. Jiang, "Dynamic leader based collective intelligence for maximum power point tracking of PV systems affected by partial shading condition," *Energy Convers. Manage.*, vol. 179, pp. 286–303, Jan. 2019.

[3] Y. Xiao, J. Ouyang, X. Xiong, Y. Wang, and Y. Luo, "Fault protection method of single-phase break for distribution network considering the influence of neutral grounding modes," *Protection Control Modern Power Syst.*, vol. 5, no. 1, pp. 111–123, Dec. 2020.

[4] Z. Bo, X. Lin, Q. Wang, Y. Yi, and F. Zhou, "Developments of power system protection and control," *Protection Control Modern Power Syst.*, vol. 1, no. 1, pp. 1–8, 2016.
[5] Z. Yao, Q. Zhang, P. Chen, and Q. Zhao, "Research on fault diagnosis for MMC-HVDC systems," *Protection Control Modern Power Syst.*, vol. 1, no. 1, pp. 1–7, Dec. 2016.
[6] Z. Li and H. Tan, "New scheme of UHVDC transmission line protection based on chebyshev window filter," *J. Eng.*, vol. 2017, no. 13, pp. 935–939, Jan. 2017.
[7] Y. Yang, N. Tai, C. Fan, L. Yang, and S. Chen, "Resonance frequency-based protection scheme for ultra-high-voltage direct-current transmission lines," *IET Gener., Transmiss. Distrib.*, vol. 12, no. 2, pp. 318–327, Jan. 2018.
[8] J. Liu, C. Fan, W. Huang, and N. Tai, "Protection scheme for high-voltage direct-current transmission lines based on transient AC current," *IET Gener., Transmiss. Distrib.*, vol. 9, no. 16, pp. 2633–2643, Dec. 2015.
[9] G. Song, J. Hou, B. Guo, and Z. Chen, "Pilot protection of hybrid MMC DC grid based on active detection," *Protection Control Modern Power Syst.*, vol. 5, no. 1, pp. 82–96, Dec. 2020.
[10] T. Bi, S. Wang, and K. Jia, "Single pole-to-ground fault location method for MMC-HVDC system using active pulse," *IET Gener., Transmiss. Distrib.*, vol. 12, no. 2, pp. 272–278, Jan. 2018.
[11] J. He, K. Chen, M. Li, Y. Luo, C. Liang, and Y. Xu, "Review of protection and fault handling for a flexible DC grid," *Protection Control Modern Power Syst.*, vol. 5, no. 1, pp. 151–165, Dec. 2020.
[12] J. Lee, D. Kang, and J. Lee, "A study on the improved capacitor voltage balancing method for modular multilevel converter based on hardware-in-the-loop simulation," *Electronics*, vol. 8, no. 10, p. 1070, Sep. 2019.
[13] L. Jiang, Q. Chen, and L. Wang, "Novel protection method for VSC-HVDC line," *J. Eng.*, vol. 2019, no. 16, pp. 2142–2146, 2019.
[14] B. Junior, L. Rui, V. Albernaz, and R. M. Monaro, "Selective non unit protection technique for multi-terminal VSC-HVDC grids," *IEEE Trans. Power Del.*, vol. 33, no. 5, pp. 2106–2114, Sep. 2018.
[15] F. Tao, Z. Xie, J. Cheng, C. Li, L. Zhao, and J. Wen, "Fast valve power loss evaluation method for modular multi-level converter operating at high-frequency," *Protection Control Modern Power Syst.*, vol. 1, no. 1, pp. 1–11, Dec. 2016.
[16] M. H. Rahman, L. Xu, and L. Yao, "Protection of large partitioned MTDC networks using DC-DC converters and circuit breakers," *Protection Control Modern Power Syst.*, vol. 1, no. 1, pp. 1–9, Dec. 2016.
[17] V. Akhmatov, M. Callavik, C. M. Franck, S. E. Rye, T. Ahndorf, M. K. Bucher, H. Muller, F. Schettler, and R. Wiget, "Technical guidelines and prestandardization work for first HVDC grids," *IEEE Trans. Power Del.*, vol. 29, no. 1, pp. 327–335, Feb. 2014.
[18] Z. Zheng, T. Tai, J. S. Thorp, and Y. Yang, "A transient harmonic current protection scheme for HVDC transmission line," *IEEE Trans. Power Del.*, vol. 27, no. 4, pp. 2278–2285, Oct. 2012.
[19] J. Liu, N. Tai, C. Fan, and Y. Yang, "Transient measured impedance-based protection scheme for DC line faults in ultra high-voltage direct-current system," *IET Gener., Transmiss. Distrib.*, vol. 10, no. 14, pp. 3597–3609, Nov. 2016.
[20] S. Gao, X. Jin, Z. Ma, and G. Song, "Novel pilot protection principle for high-voltage direct current transmission lines based on fault component current characteristics," *IET Gener., Transmiss. Distrib.*, vol. 9, no. 5, pp. 468–474, Apr. 2015.
[21] H. Xiao, Y. Li, R. Liu, and X. Duan, "Single-end time-domain transient electrical signals based protection principle and its efficient setting calculation method for LCC-HVDC lines," *IET Gener., Transmiss. Distrib.*, vol. 11, no. 5, pp. 1233–1242, 2017.
[22] F. Kong and B. Zhang, "A hybrid protection scheme based on integrated impedance for 800kV UHVDC transmission line," in *Proc. 12th IET Int. Conf. Develop. Power Syst. Protection (DPSP)*, 2014, doi: 10.1049/cp.2014.0106.
[23] L. Tang, X. Dong, S. Shi, and Y. Qiu, "A high-speed protection scheme for the DC transmission line of a MMC-HVDC grid," *Electr. Power Syst. Res.*, vol. 168, pp. 81–91, Mar. 2019.
[24] X. Liu, A. H. Osman, and O. P. Malik, "Hybrid traveling wave/boundary protection for monopolar HVDC line," *IEEE Trans. Power Del.*, vol. 24, no. 2, pp. 569–578, Feb. 2009.
[25] B. Li, Y. Li, J. He, and W. Wen, "A novel single-ended transient-voltage-based protection strategy for flexible DC grid," *IEEE Trans. Power Del.*, vol. 34, no. 5, pp. 1925–1937, Oct. 2019.
[26] Y. Xu, J. Liu, and Y. Fu, "Fault-line selection and fault-type recognition in DC systems based on graph theory," *Protection Control Modern Power Syst.*, vol. 3, no. 1, pp. 267–276, Dec. 2018.
[27] F. Zhang and L. Mu, "New protection scheme for internal fault of multi-microgrid," *Protection Control Modern Power Syst.*, vol. 4, no. 1, pp. 159–170, Dec. 2019.
[28] B. Li, J. He, Y. Li, and B. Li, "A review of the protection for the multi-terminal VSC-HVDC grid," *Protection Control Modern Power Syst.*, vol. 4, no. 1, pp. 239–249, Dec. 2019.
[29] G. Song, Z. Chang, C. Zhang, S. T. H. Kazmi, and W. Zhang, "A high speed single-ended fault detection method for DC distribution feeder—Part I: Feasibility analysis of magnetic ring as line boundary," *IEEE Trans. Power Del.*, vol. 35, no. 3, pp. 1249–1256, Jun. 2020.
[30] T. Wang, G. Song, and K. S. T. Hussain, "Adaptive single-pole auto-reclosing scheme for hybrid MMC-HVDC systems," *IEEE Trans. Power Del.*, vol. 34, no. 6, pp. 2194–2203, Dec. 2019.
[31] G. Song, T. Wang, and K. S. T. Hussain, "DC line fault identification based on pulse injection from hybrid HVDC breaker," *IEEE Trans. Power Del.*, vol. 34, no. 1, pp. 271–280, Feb. 2019.
[32] S. Xue, J. Lian, J. Qi, and B. Fan, "Pole-to-ground fault analysis and fast protection scheme for HVDC based on overhead transmission lines," *Energies*, vol. 10, no. 7, p. 1059, Jul. 2017.
[33] J. Yu, Z. Zhang, Z. Xu, and G. Wang, "An equivalent calculation method for pole-to-ground fault transient characteristics of symmetrical monopolar MMC based DC grid," *IEEE Access*, vol. 8, pp. 123952–123965, 2020.
[34] G. Song, J. Luo, S. Gao, X. Wang, and K. Tassawar, "Detection method for single-pole-grounded faulty feeder based on parameter identification in MVDC distribution grids," *Int. J. Electr. Power Energy Syst.*, vol. 97, pp. 85–92, Apr. 2018.
[35] H. Shu, N. An, B. Yang, Y. Dai, and Y. Guo, "Single pole-to-ground fault analysis of MMC-HVDC transmission lines based on capacitive fuzzy identification algorithm," *Energies*, vol. 13, no. 2, p. 319, Jan. 2020.
[36] C. Zhao, X. Chen, C. Cao, and H. Jing, "Control and protection strategies for MMC-HVDC under DC faults," *Autom. Electr. Power Syst.*, vol. 35, no. 23, pp. 82–87, 2011.
[37] F. Badrkhani Ajaei and R. Iravani, "Cable surge arrester operation due to transient overvoltages under DC-side faults in the MMC–HVDC link," *IEEE Trans. Power Del.*, vol. 31, no. 3, pp. 1213–1222, Jun. 2016.
[38] P. Ahlgren, B. Jarneving, and R. Rousseau, "Requirements for a cocitation similarity measure, with special reference to Pearson's correlation coefficient," *J. Amer. Soc. Inf. Sci. Technol.*, vol. 54, no. 6, pp. 550–560, Apr. 2003.

**NA AN** was born in Hebei, China, in 1985. She received the master's degree from the Kunming University of Science and Technology, Kunming, China, where she is currently pursuing the Ph.D. degree.

Her research interests include power transmission and transformation equipment and automation.

**HONGCHUN SHU** (Member, IEEE) received the Ph.D. degree in electrical engineering from the Harbin Institute of Technology, Harbin, China, in 1997.

He is currently a Professor and the Vice President with the Kunming University of Science and Technology. His research interests include protective relay, fault location, and distribution networks. He is a Senior Member of the Chinese Society for Electrical Engineering.

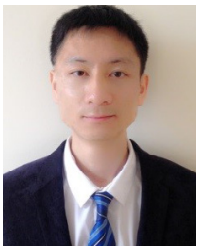

**BO YANG** received the B.Eng. degree in electrical engineering from the South China University of Technology, Guangzhou, China, in 2010, and the Ph.D. degree in electrical engineering from the University of Liverpool, Liverpool, U.K., in 2015.

He is currently an Associate Professor with the Faculty of Electric Power Engineering, Kunming University of Science and Technology. His research interests include nonlinear adaptive control, meta-heuristic algorithms, and renewable energy optimization and control.

**PULIN CAO** (Member, IEEE) received the B.Eng. degree in electrical engineering from the South China University of Technology, Guangzhou, China, in 2010, and the Ph.D. degree in electrical engineering from the Kunming University of Science and Technology, Kunming, China, in 2015.

He is currently an Associate Professor with the Faculty of Electric Power Engineering, Kunming University of Science and Technology. His current research interests include fault location, overvoltage, and data fusion.

**JIAN SONG** received the master's degree from the Kunming University of Science and Technology, Kunming, China, in 2009, where he is currently pursuing the Ph.D. degree.

His research interests include power system signal processing, and complex system modeling and control.

**YU GUO** (Member, IEEE) received the Ph.D. degree in mechatronic engineering from Chongqing University, Chongqing, China, in 2003.

He is currently a Professor with the Kunming University of Science and Technology. His research interests include mechanical dynamic and vibration analysis.